Front. Earth Sci. 2019, 13(4): 682–694
https://doi.org/10.1007/s11707-019-0803-7

RESEARCH ARTICLE

Cloud-based typhoon-derived paddy rice flooding and lodging detection using multi-temporal Sentinel-1&2

Wanben WU[1], Wei WANG[1], Michael E. Meadows[1,3], Xinfeng YAO[4], Wei PENG (✉)[2]

1 School of Geographic Sciences, East China Normal University, Shanghai 200241, China
2 Information Technology Services Office, East China Normal University, Shanghai 200241, China
3 Department of Environmental & Geographical Science, University of Cape Town, Cape Town 7701, South Africa
4 Shanghai Academy of Agricultural Sciences, Shanghai 201403, China

Abstract Rice production in China's coastal areas is frequently affected by typhoons, since the associated severe storms, with heavy rain and the strong winds, lead directly to the rice plants becoming flooded or lodged. Long-term flooding and lodging can cause a substantial reduction in rice yield or even destroy the harvest completely. It is therefore urgent to obtain accurate information about paddy rice flooding and lodging as soon as possible after the passing of the storm. This paper proposes a workflow in Google Earth Engine (GEE) for mapping the flooding and lodging area of paddy rice in Wenzhou City, Zhejiang, following super typhoon Maria (Typhoon No.8 in 2018). First, paddy rice in the study area was detected by multi-temporal Sentinel-1 backscatter data combined with Sentinel-2-derived Normalized Difference Vegetation Index (*NDVI*) using the Random Forests (RFs) algorithm. High classification accuracies were achieved, whereby rice detection accuracy was calculated at 95% (VH + *NDVI*-based) and 87% (VV + *NDVI*-based). Secondly, Change Detection (CD) based Rice Normalized Difference Flooded Index (*RNDFI*) and Rice Normalized Difference Lodged Index (*RNDLI*) were proposed to detect flooding and lodged paddy rice. Both *RNDFI* and *RNDLI* were tested based on four different remote sensing data sets, including the Sentinel-1-derived VV and VH backscattering coefficient, Sentinel-2-derived *NDVI* and Enhanced Vegetation Index (*EVI*). Overall agreement regarding detected area between the each two different data sets was obtained, with values of 79% to 93% in flood detection and 64% to 88% in lodging detection. The resulting flooded and lodged paddy rice maps have potential to reinforce disaster emergency assessment systems and provide an important resource for disaster reduction and emergency departments.

Keywords typhoons, paddy rice, flooding, lodging, Sentinel-1, Sentinel-2, Google Earth Engine

1 Introduction

As a major natural hazard affecting coastal areas, typhoons have serious impacts on agriculture. The heavy rains and wind brought by typhoons have a direct impact on agricultural production in the affected areas. For example, there are on average 6.25 typhoons that make landfall on the coast of China every year and annual economic losses due to typhoon landfall amount to RMB 200 million (Liu et al., 2009). Hence, accurate emergency disaster monitoring is of key importance to ensure food security.

Over the past three decades, remote sensing technology has developed rapidly, with an increase in availability of remote sensing data such as Landsat-5, MODIS, Landsat-7, Landsat-8, Sentinel-1 and Sentinel-2 data sets which are accessible free of charge. Furthermore, cloud-based computing platforms, such as Google Earth Engine (GEE), can complete the integration and analysis of huge geospatial and remote sensing data sets related to the object of study within a very short period of time (Mateo-García et al., 2018). As a remote sensing cloud computing platform, GEE can easily realize the integrated processing of remote sensing data and geospatial information acquisition, analysis and mapping under large spatial and long temporal scale. For example, high-resolution mapping of global surface water and forest cover products based on GEE have been produced in recent years (Pekel et al., 2016; Hansen et al., 2013). In addition, a global and consistent evaluation of coastal erosion and accretion over

Received January 2, 2019; accepted October 9, 2019

E-mail: wpeng@admin.ecnu.edu.cn

32 years, based on GEE, has been proposed (Mentaschi et al., 2018). Given the enormous computational load required in using these products, they would not be feasible without GEE. Pixel-based processing is facilitated in GEE, resolving the problem of cloud removal in complex weather conditions, and thereby greatly improving the use efficiency of remote sensing images.

Accordingly, remote sensing has been broadly used in near-real time assessment of natural hazards that affect crops, including flooding and lodging. Flooding in rice fields means excess of water inhibiting rice growth or even completely submerged, which occur because of unexpected rainfall, excessive river flow, cyclonic storms and tidal surge (Sakagami and Kawano, 2011). While lodging here refers to the rice plants are permanent displacement of the stems from their upright position, when lodging occurs, the canopy structure would be destroyed, and the capacity of photosynthetic rate and dry matter production sharply reduced (Setter et al., 1997). Specifically, optical remote sensing data are now widely used in crop disaster research. For example, Landsat TM reflectance before and after flooding has been used to assess the change in the distribution of surface water and to obtain accurate information about the extent of flooded areas (Wang et al., 2002). Furthermore, by incorporating the Digital Elevation Model (DEM), Wang et al. (2002) were able to greatly improve estimation accuracy by also identifying flooded areas under the forest canopy. Rice fields damaged by flooding were also detected using MODIS-derived indices, including Modified Land Surface Water Index (Kwak et al., 2015) and Global Land Cover data sets by National Mapping Organizations (GLCNMO 2008). By doing so, they were able to produce a map indicating the distribution of flooded rice fields across the entire country of Bangladesh for July–August 2007 (Kwak et al., 2015). Unmanned aerial vehicle (UAV) technology is increasingly being applied to natural hazard research. For example, the UAV-obtained imagery with a digital surface model (DSM) was deployed to propose a spectral hybrid image classification and decision tree method that was able to detect rice lodging in Taiwan, China (Yang et al., 2017).

However, optical remote sensing data rely on cloud-free (or largely cloud-free) imagery, so it is unsuited to conditions associated with natural hazards such as intense storms. Synthetic Aperture Radar (SAR) sensors, on the other hand, can be applied in almost any weather conditions, or during the night (Mutanga and Kumar, 2019). SAR is therefore invaluable for disaster assessment under the kind of extreme meteorological conditions that characterize typhoons. In addition, Sentinel-1 has a shorter return period (6–12 days) and high spatial resolution (10 m), which better meets the needs of disaster research. For instance, Lee and Lee (2003) collected temporal Radarsat SAR images before, during, and after a flood event to evaluate post-flooding conditions in paddy rice fields, and they also classified the rice fields in flooding and post-flooding recovery conditions. Meanwhile, several studies on crop lodging have been based on microwave data. Bouman and Hoekman (1993), for example, designed a backscatter change detection experiment for lodging in winter wheat across six different spectral bands which revealed that lodging increased backscatter in all cases.

Previous studies have mainly used the CD detection method to obtain only a single type of crop damage, such as flooding or lodging. However, given that rice flooding and lodging occur simultaneously in a typhoon, a method of assessing the extent of both types of damage at the same time is needed. Previous studies have been restricted to small-scale field trials for the extraction of rice lodging, and a method for assessing the problem of rice lodging at a larger spatial scale has not been developed until now. The main purpose of this study, therefore, is to propose a method based on Earth Observation (EO) big data, using the GEE cloud computing platform, to extract simultaneous rice lodging and flooding distribution following the passage of a typhoon.

2 Materials and methods

2.1 Study area

In this study, Typhoon Maria (number eight in 2018) was chosen as a research case; the typhoon made landfall on the coast of Fujian, on 11 July 2018 (Tian and Zou, 2018). Based on the track of typhoon Maria and its area of impact, we selected the coastal city of Wenzhou in Zhejiang as the study area. The maximum cumulative rainfall during the typhoon period was 300 mm, and the maximum recorded wind speed reached 42 m/s. Maria had a very serious impact on agricultural production in Wenzhou, causing a large number of early-season rice paddies to be flooded and lodged, affecting an area of 15220 ha and resulting in a direct economic loss of RMB 10924.9 million. The location of the study area is shown in Fig. 1. Wenzhou covers an area of 1206100 ha, of which 27446.67 ha is utilized for early-season rice (Xia and Wu, 2017).

2.2 Data sets

2.2.1 Radar imagery

Sentinel-1 provides data from a dual-polarization C-band SAR sensor, which are available from October 2014 with a revisit interval of six days at a spatial resolution of 10 m. In this paper, we used multi-temporal Sentinel-1 data to estimate both paddy rice distribution and flooding extent. Detailed information regarding Sentinel-1 data used in this study is presented in Table 1.

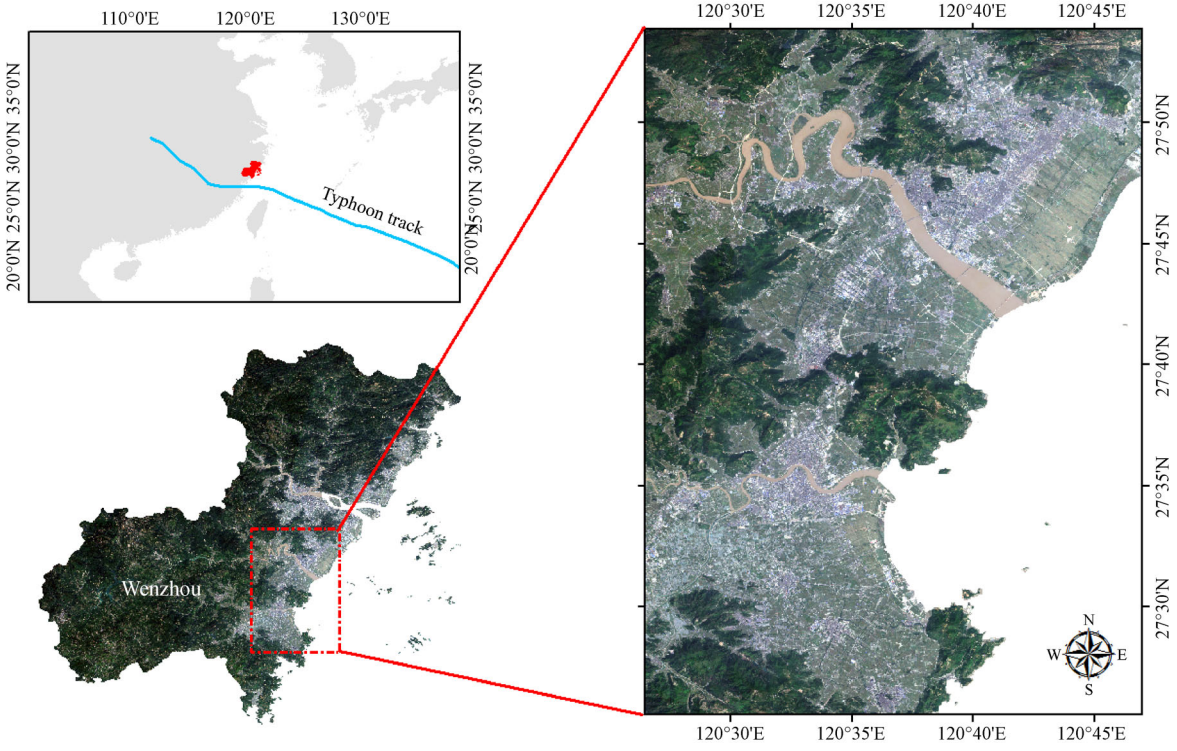

Fig. 1 Location of the study area with true color visualization of Sentinel-2 data, whereby the blue line represents the track of Typhoon Maria.

Table 1 Characteristics of Sentinel-1 GRD IW images used in this paper

Sensor	Date	Scenes	Event	Obit / Pol	Application
Sentinel-1 (C) GRDH 10 m	08-May-2016	4		Ascending (VV VH)	Paddy rice mapping
	19-July-2016	4			
	12-Aug-2016	4			
	13-July-2015	4	Reference	Ascending (VV VH)	Flooding and lodging paddy rice detection
	19-July-2016	4			
	14-July-2017	4			
	21-July-2017	4			
	16-July-2018	4	Disaster		
	21-July-2018	4			

2.2.2 Optical imagery

Sentinel-2 is a wide-swath, high-resolution, multispectral imaging mission supporting Copernicus Land Monitoring studies, including the monitoring of vegetation, soil and water cover, as well as observations of inland waterways and coastal areas (Drusch et al., 2012). Sentinel-2 samples 13 spectral bands: four bands at 10 m, six bands at 20 m and three bands at 60 m spatial resolution, with data available free of charge since 23 June 2015 on a return interval of five days. In this paper, Sentinel-2 annual data from 01 May to 01 July were used for each of the years 2015, 2016, 2017 and processed by cloud removal and median fusion to obtain cloud-clear data. Open water, urban and vegetated land covers were then identified using the supervised classification method. Finally, Multi-temporal Sentinel-2-derived *NDVI* and *EVI* series data were used to calculate *RNDFI* and *RNDLI* to detect flooded and lodged paddy rice pixels. Detailed information for the Sentinel-2 data used in this study is provided in Table 2.

2.2.3 Rice crop calendar

The Chinese National Meteorological Information Center produces a rice calendar data set which includes a range of

Table 2 Characteristics of Sentinel-2 MSI images used in this paper

Sensor	Date	Scenes	Used bands	Application
Sentinel-2 (MSI) 10 m	From 1/May To 1/July, 2015, 2016, 2017	55	B3, B4, B8, B11	Paddy rice mapping
	From 10/July to 25/July, 2016	19	B2, B4, B8	Flooding and lodging paddy rice detection
	From 10/July to 25/July, 2017			
	From 10/July to 25/July, 2018	24		

crop growth information for several agricultural stations from 1991 to present, such as crop name, growth stage and observation date.

2.2.4 Training and validation samples

To evaluate the accuracy of paddy rice distribution, randomly distributed sample points in the study area were selected for each of the land cover types by combining high-resolution Google Earth imagery, survey information, and the NLCD-2000 land cover data set. All sample points were randomly divided into two sets, one set as a classification sample and the other as a precision verification sample.

2.2.5 DEM

The digital elevation model (Shuttle Radar Topography Mission, SRTM, derived from the GEE database) and the DEM derived slope of each pixel were also calculated because they influence rice growth conditions; for paddy rice growth to be feasible, pixels need to satisfy the conditions of slope angle < 2 degrees and elevation < 2000 m (Xiao et al., 2005).

2.3 Workflow

To achieve detection of flooded and lodged paddy rice in GEE, the workflow as illustrated in Fig. 2 was designed, consisting of two main parts, including paddy rice mapping and paddy rice disaster mapping. First, based on differences in the values of backscatter coefficient and *NDVI* for paddy rice during different growth stages, we combined the multi-temporal Sentinel-1 derived VV or VH backscatter coefficient and Sentinel-2 derived *NDVI* to detect paddy rice with the help of the RFs classification algorithm. In addition, a DEM was used to improve the detection accuracy through masking the pixels for areas that would be impossible for rice cultivation. Selected land

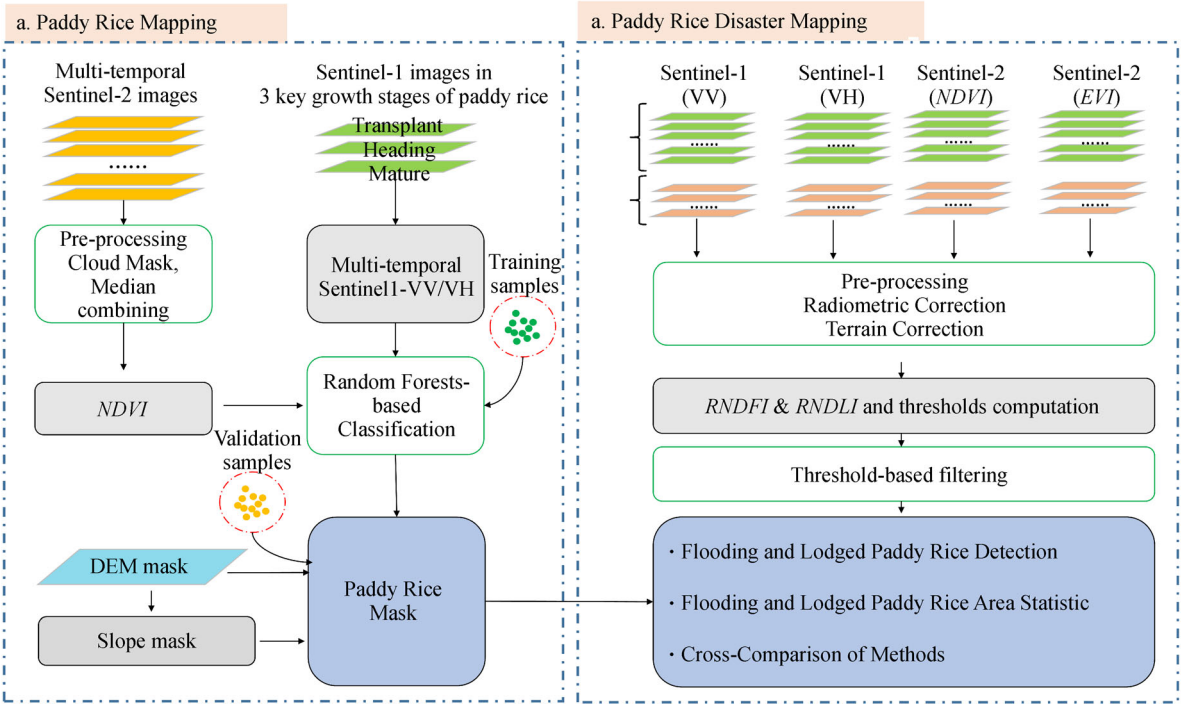

Fig. 2 The extraction method of flooded and lodged paddy rice using GEE.

cover samples were used for rice extraction and precision verification (See Fig. 2(a) for details).

Secondly, two CD-based indices were designed based on multi-temporal images, i.e. the *RNDFI* to highlight flooded paddy rice areas, and the *RNDLI* to highlight lodged paddy rice pixels. In this study, changes in both *RNDFI* and *RNDLI* were detected in GEE using the multi-temporal Sentinel-1 VV and VH backscatter coefficients and Sentinel-2 derived spectral indices of *NDVI* and *EVI*. Finally, flooded and lodged paddy rice areas based on different data sets were estimated using the appropriate thresholds of CD-based indices, and the results were compared to evaluate wider application of the method in typhoon prone regions (See Fig. 2(b) for details).

2.3.1 The GEE platform

As a cloud-based platform for planetary-scale geospatial analysis, GEE plays an increasingly key role in research related to a wide range of environmental issues, including those that have significant impacts on human society. These include deforestation, water management, climate change, land degradation, biodiversity conservation, and disaster risk management and mitigation (Hansen et al., 2013; Pekel et al., 2016). GEE allows users to collect and utilize multi-source remote sensing data, including MODIS, Sentinel-1, Sentinel-2, Landsat 4-5, Landsat 7, Landsat 8, etc. on a single analytical platform. In addition, GEE can process, analyze, map and export results within a very short time, typically from just seconds to a few minutes (go to Earthengine Google website for further details). In this paper, all remote sensing data were compiled from the database in GEE, including the Sentinel-1 backscatter coefficient data, composed cloud-free Sentinel-2 multi-band data, as well as the global 30 m DEM data set. To unify the resolution of the data, we applied the Kriging interpolation method to unify the resolution of all products used in this study to 10 m.

2.3.2 Paddy rice mapping

A phenology- and pixel-based algorithm was used for paddy rice mapping applying the following two steps.

1) Rice detection method

In different growth stages, backscattering coefficients of rice plants are significantly different (Nquyen et al., 2016). As the crop develops from the transplanting phase, the backscattering coefficient increases and reaches its maximum around the heading phase, then declines steadily during the maturity phase, and reaches its lowest value after harvesting (Fig. 3). Based on this feature and the calendar for rice growth in the study area (Fig. 4), we selected Sentinel-1 polarization data in three different rice growth phases (transplanting, heading, harvesting) as rice classification data. In addition, we used the cloud-free Sentinel-2 derived *NDVI* in the rice heading phase to improve the accuracy of paddy rice detection (Lasko et al., 2018). *NDVI* can be calculated according to Eq. (1). Figure 5 illustrates the layer stack results under two polarization modes in false color. In GEE, there are various classifiers available for users, including decision tree, Random Forests (RFs), Classification and Regression Tree (CART), Support Vector Machine (SVM), etc. (Gorelick et al., 2017). There are several studies that use RFs for classifying SAR data (Balzter et al., 2015; Fu et al., 2017). Furthermore, previous study also evaluated the performance of SVM and RFs classifiers for rice crop mapping using multi-temporal Sentinel-1 VH polarization data, and their results showed that RFs were more accurate than SVM (Son et al., 2017). Thus, we selected RFs to classify

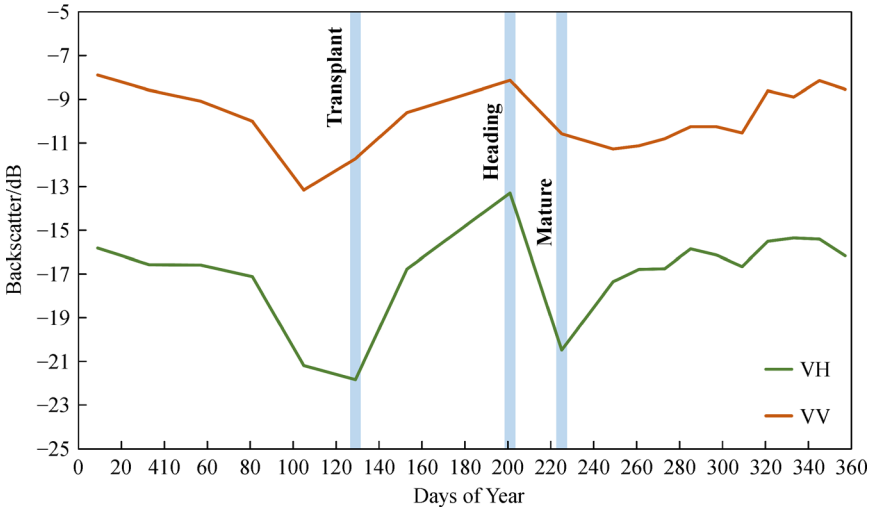

Fig. 3 Temporal backscatter profiles at VH and VV polarizations of various rice growth stages acquired for the 2016 rice-growing season for selected sites in Wenzhou, Zhejiang.

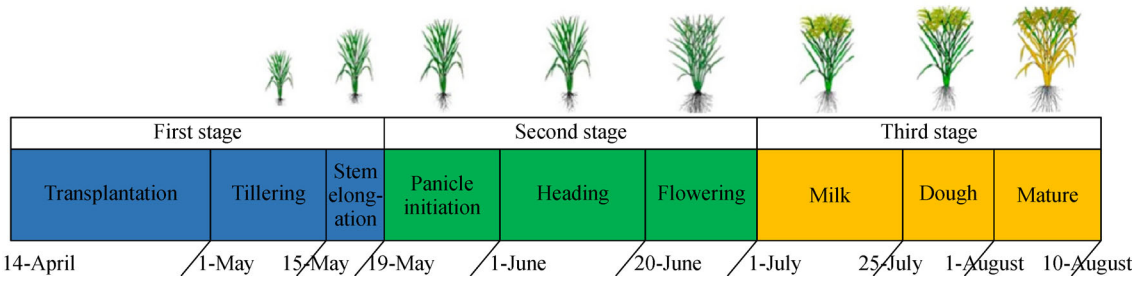

Fig. 4 Rice phenology calendar in Zhejiang.

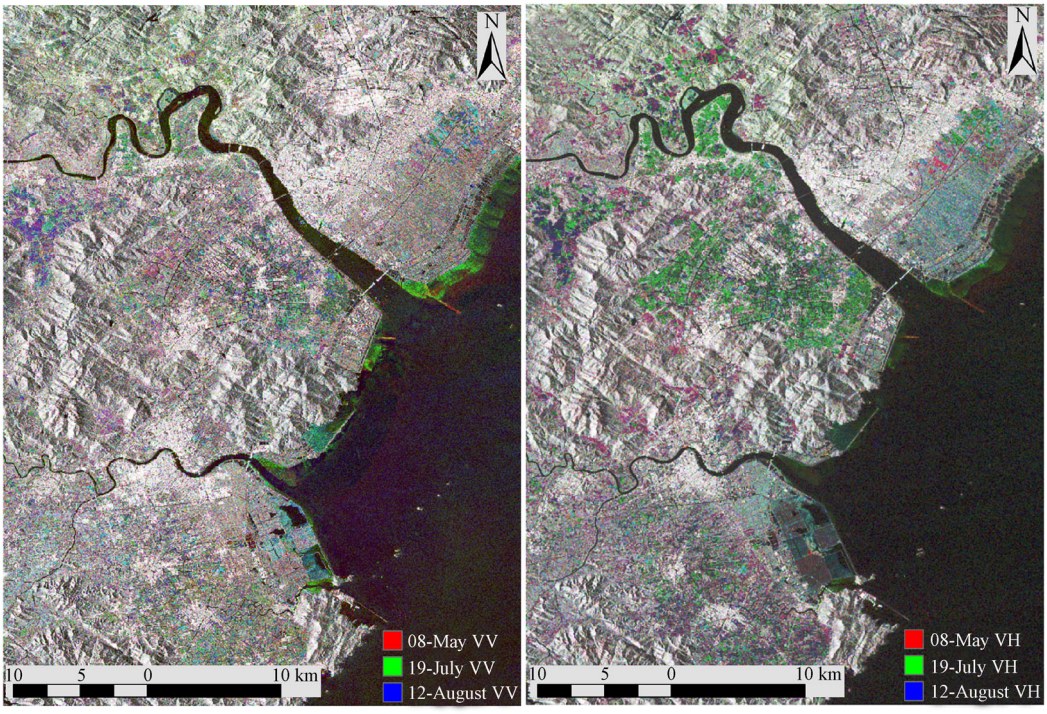

Fig. 5 Multi-temporal SAR composite in (a) VV and (b) VH polarization.

the land cover in the study area, with the following categories: paddy rice, water, urban, forest, and other land use.

The specific formulas of *NDVI* and *EVI* are as follows:

$$NDVI = (\mathrm{NIR}-\mathrm{R})/(\mathrm{NIR}+\mathrm{R}), \quad (1)$$

$$EVI = 2.5(\mathrm{NIR}-\mathrm{R})/(\mathrm{NIR}+6\mathrm{R}-7.5\mathrm{B}+1), \quad (2)$$

where NIR is the near infrared band corresponding to Sentinel-2 band 8 (Sentinel-2A: 835.1 nm/Sentinel-2B: 833 nm), R is the red band, corresponding to Sentinel-2 band 4 (Sentinel-2A: 664.5 nm/Sentinel-2B: 665 nm), and B indicates blue band, corresponding to Sentinel-2 band 3 (Sentinel-2A: 496.6 nm/Sentinel-2B: 492.1 nm).

2) Post processing

The DEM and slope data sets were used to remove pixels whose elevation and slope do not meet the conditions for rice planting, which has the advantage of reducing the effect of terrain, such as mountain shadow, on Sentinel-1 data acquisition, thereby minimizing rice misdetection resulting from poor data quality. For this reason, the pixels with elevation above 2000 m or slope angles greater than 2 degrees were removed from the rice extraction results obtained (Xiao et al., 2005). After reducing the terrain effect, the outputs were then filtered using two steps aimed at accounting for two further possible sources of error. First, the image was filtered by a morphological procedure; opening the filter enlarges the boundary of regions of the foreground pixels, and closing filter which removes small holes while preserving boundaries. Both filters use 5 × 5 pixel windows. Secondly, clusters smaller than 5 pixels were excluded to remove the areas that were likely not to be paddy fields.

These post-processing steps effectively reduce the effect of data noise on rice extraction results.

3) Accuracy assessment

The various land cover type samples were assessed for post-classification accuracy. A confusion matrix was constructed, from which the producer's accuracy (PA), user's accuracy (UA), overall classification accuracy (OA) and Kappa (statistic) index of the paddy field mapping were calculated.

2.3.3 Paddy field flooding and lodging area detection

1) *RNDFI* and *RNDLI* extraction

As in the algorithm produced by Cian et al. (2018), the Normalized Difference Flood Index (*NDFI*) was proposed to highlight decreased backscattering values in flooded pixels, while the Normalized Difference Flood in short Vegetation Index (*NDFVI*) was proposed to detect increased backscattering values in pixels that are shallow water flooded in short vegetation. Using the statistics derived from the multi-temporal images, the *NDFI* and *NDFVI* were computed:

$$NDFI = \frac{\text{mean } \sigma_0(\text{“reference”}) - \text{min } \sigma_0(\text{“reference + flood”})}{\text{mean } \sigma_0(\text{“reference”}) + \text{min } \sigma_0(\text{“reference + flood”})}, \tag{3}$$

$$NDFVI = \frac{\text{max } \sigma_0(\text{“reference + flood”}) - \text{mean } \sigma_0(\text{“reference”})}{\text{max } \sigma_0(\text{“reference + flood”}) + \text{mean } \sigma_0(\text{“reference”})}, \tag{4}$$

where “reference” means the image collection in unflooded conditions and “reference + flood” means the collection contains the images both in flooded and unflooded conditions.

The backscattering coefficient decreases sharply once the rice is flooded (Wakabayashi et al., 2019). When rice lodging occurs, the proportion of rice leaf area increases, and the backscattering coefficient increases due to the secondary scattering effect caused by shallow water in short vegetation and additional scattering from rice that appears to have greater leaf area (Cian et al., 2018). Thus, lodging and flooding events can be effectively identified by identifying the larger or smaller backscatter coefficient. However, the *NDFI* and *NDFVI* were designed for short vegetation, we improved these indices to better deal with flooded and lodged detection in paddy rice fields designed as follows. First, because of the rice planting system in the study area, flooding occurs in the pre-transplanting period. If the data acquisition time is not controlled, it is possible to misclassify the pre-transplanting as a flooding event, resulting in the overestimation of flooded areas. Secondly, because of the obvious noise characteristics of SAR data (Torres et al., 2012), the median value for pixels more accurately represents the general value when multi-temporal pixel values are counted, which effectively eliminates the influence of outliers on the statistical results. In view of the above problems, the following two improvements have been made in the calculation of the proposed indices:

i) To exclude the impact of rice transplanting and harvesting events on the results of our indices calculation, the rice growth time that corresponds to a near disaster-free year was used as the reference data.

ii) The median value of the backscattering rate was used instead of the original mean value in order to eliminate the influence of noise and abnormal outlier values on the results.

As summarized in Fig. 2, two multi-temporal SAR and Sentinel-2 series collections were created, whereby the “normal” set represents the data set collection obtained in non-typhoon effected period, while the “normal + disaster” set, that contains images of both the “normal” and typhoon-effected-season data sets. Details of data sets used in this study is shown in Table 1 and Table 2. Based on the above two data sets, the time series in each set were analyzed statistically through the calculation of the maximum, minimum and median of each pixel for both data sets. Accordingly, in order to distinguish our proposed indices from those developed in previous studies (Cian et al., 2018), we defined the Rice Normalized Flooding Index (*RNDFI*) for flooded rice detection, and the Rice Normalized Lodged Index (*RNDLI*) for lodged rice detection, which were calculated as follows:

$$RNDFI = \frac{\text{median } \sigma_0(\text{“normal”}) - \text{min } \sigma_0(\text{“normal + disaster”})}{\text{median } \sigma_0(\text{“normal”}) + \text{min } \sigma_0(\text{“normal + disaster”})}, \tag{5}$$

$$RNDLI = \frac{\text{max } \sigma_0(\text{“normal + disaster”}) - \text{median } \sigma_0(\text{“normal”})}{\text{max } \sigma_0(\text{“normal + disaster”}) + \text{median } \sigma_0(\text{“normal”})}, \tag{6}$$

where median σ_0(“normal”) represents the median value of multi-temporal backscatter of rice in non-typhoon-effected season, min σ_0(“normal + disaster”) represents the lowest backscatter value under the typhoon-effected condition, and max σ_0(“normal + disaster”) represents the highest backscatter value in the typhoon-effected condi-

tion. High values of *RNDFI* indicate flooded paddy rice, while high values of *RNDLI* indicate lodged paddy rice.

2) *RNDLI* and *RNDFI* change detection

Based on the generated paddy rice map and the two indices, we next detected the flooded and lodged areas of paddy fields using the CD method. Referring to the threshold calculation method proposed by Long et al. (2014), we extracted the flooding and lodged paddy rice pixels using the criteria as in Eqs. (7) and (8) below.

Specifically, in the case of extracting the flooded pixels, the threshold criterion in the CD method is simply that the pixel value of *RNDFI* is greater than the mean pixel value minus the standard deviation of the entire image multiplied by a coefficient k_F.The value of k_F was set as 1.5 for this case based on previous research (Long et al., 2014; Cian et al. 2018).

$$P_F > \text{mean}(RNDFI) - k_F \text{std}(RNDFI). \quad (7)$$

The identification of lodging in paddy pixels needs to meet the following two conditions:

i) The pixel does not conform to Eq. (8), that is non-flooding pixels.

ii) The pixel value of *RNDLI* is greater than the mean pixel value plus the standard deviation of the entire image multiplied by a coefficient k_L. The optimal value of k_L was set to be 1.5 for this study based on the previous research (Long et al., 2014; Cian et al., 2018).

$$P_L > \text{mean}(RNDLI) + k_L \text{std}(RNDLI). \quad (8)$$

3) *NDVI* and *EVI* change detection

For further comparison, multi-temporal Sentinel-2-derived *NDVI* and *EVI* time series were also used to calculate *RNDFI* and *RNDLI*, and also used to detect flooded and lodged paddy rice pixels, respectively. *NDVI* and *EVI* can be calculated according to Eqs. (1) and (2). All the reference Sentinel-2 images were obtained from a year close to the original and in the same paddy rice growth period. All the Sentinel-2 data used in this study were processed with cloud-masking, radiometric calibration and atmospheric correction to produce clear-sky surface reflectance data. Further extraction of flooded and lodged rice pixels followed the threshold criterion technique in Sentinel-1 backscatter-based flooding detection method.

4) Disaster area agreement evaluation

To compare the flooding and lodging area detection results, we further conducted cross-comparison of differences among any two data set-based methods in nine regions of Wenzhou City, the agreement can be calculated using Eq. (9).

$$\text{Agreement} = \frac{S_{\text{agree}}}{S_{\text{total}}} \times 100\%, \quad (9)$$

where S_{agree} is the area of flooded or lodged region in both compared maps, S_{total} is the area of all compared pixels.

3 Results

3.1 Mapped paddy rice

The two paddy rice maps generated from VV + *NDVI*-based and VH + *NDVI*-based are shown in Fig. 6. The mapped areas for early paddy rice detection using two methods are shown in Table 3. Government statistics for 2016 indicate that 27446.7 ha early paddy rice was planted in the study region (Xia and Wu, 2017), while the VV + *NDVI* derived paddy rice area is 29798 ha (8.6% more than reported in government statistics), and the VH + *NDVI* derived paddy rice area yielded 23973.4 ha (12.7% less than reported in government statistics).

3.2 Accuracy assessment of paddy rice mapping

In this section, confusion matrices are provided in order to evaluate the accuracy of the two classification results. Overall, producer and user accuracies were calculated using the unbiased areal estimates. Further details about the confusion matrices and calculated accuracies are shown in Table 4, The classification results yield accuracies of 93% (VH + *NDVI*) and 85% (VV + *NDVI*), and kappa statistical values are 0.9 (VH + *NDVI*) and 0.8 (VV + *NDVI*). We further merged the classification results into rice and non-rice, and found that the accuracies of rice extraction based on data sets of VH + *NDVI* and VV + *NDVI* were 95% and 87%, respectively. In general, accuracy of the VH + *NDVI*-based paddy detection exceeds that of the VV + *NDVI*-based result. This has been attributed to the fact that VV is more affected by standing water in fields, and the signal is attenuated by the vertical structure of rice plants (Bouvet et al., 2009), while VH is less affected (Nguyen et al., 2016). These results are also consistent with previous findings (Lasko et al., 2018). Therefore, VH + *NDVI*-derived paddy rice maps were used in rice disaster assessment in this paper.

3.3 Disaster mapping

In all, 16 scenes from Sentinel-1 data were used as reference images, and eight scenes from Sentinel-1 data were used to represent disaster conditions (Table 1). Meanwhile, a total of 19 scenes from Sentinel-1 data were used as reference images (Table 1), and 20-four scenes from Sentinel-2 data were used to represent disaster conditions (Table 2). Thereafter, employing CD-based method in Section 2.3.3, *RNDFI* and *RNDLI* developed by four types of data sets were used to identify the flooded and lodged areas in paddy rice fields and to produce the rice disaster maps, respectively. Figures 7(a) and 7(b) show the results for VV-based and VH-based disaster detection, while Figs. 7(c) and 7(d) show the results for *NDVI*-based and *EVI*-based disaster detection.

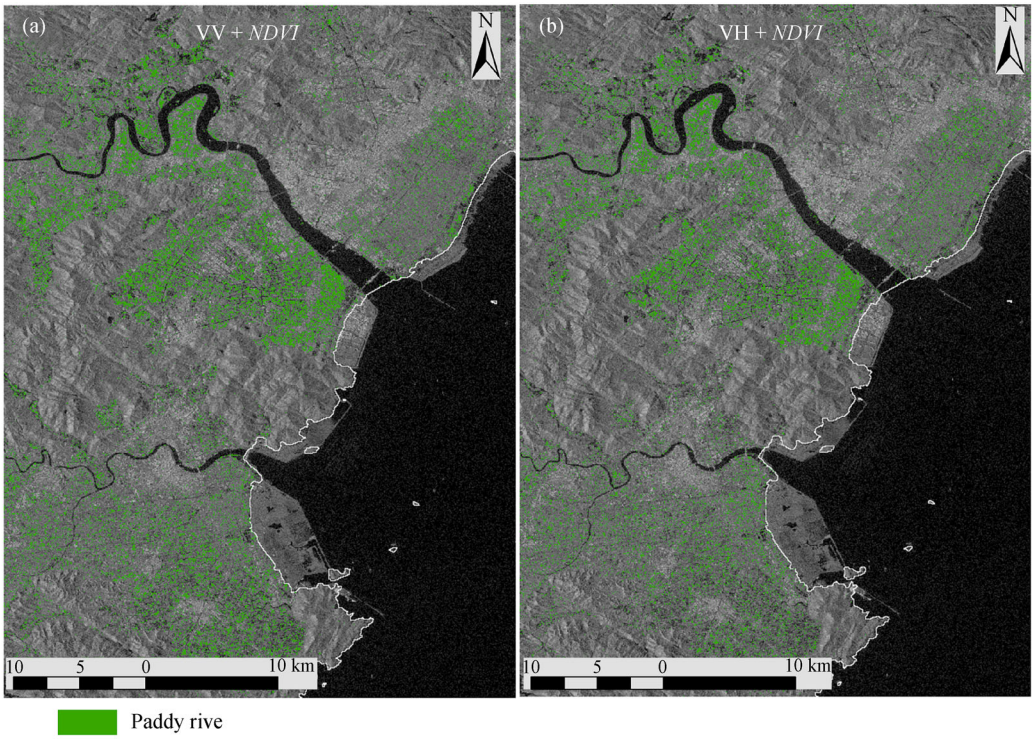

Fig. 6 Results of paddy detection using (a) the VV + *NDVI* based method, (b) the VH + *NDVI* based method.

Table 3 Paddy rice area of nine regions in the study region based on two data sets

Region	Area ha	
	VV + *NDVI*	VH + *NDVI*
Cangnan	5721.9	4367.91
Ouhai	1872.1	1712.27
Pingyang	5286.4	4162.51
Ruian	7478.7	6654.26
Taishun	795.98	414.51
Wencheng	671.88	424.55
Wenzhou	433.54	431.02
Yongjia	2520.8	1664.39
Yueqing	5016.8	4141.96
Sum	VV + *NDVI*-based 29798	VH + *NDVI*-based 23973.4

Additional statistics on flooded and lodged paddy rice areas are provided in Figs. 8(a) and 8(b). Accordingly, the flooded paddy rice areas using different data sets in Wenzhou City were as follows: 6548.62 ha (VV-based), 6943.27 ha (VH-based), 6035.77 ha (*NDVI*-based) and 6136.99 ha (*EVI*-based). The calculated lodged paddy rice areas using different data sets were: 1851.91 ha (VV-based), 1787.22 ha (VH-based), 2120.32 ha (*NDVI*-based) and 1898.61ha (*EVI*-based). Table 5 provides statistical details about flooded and lodged rice areas in nine regions of Wenzhou.

Cross-comparison of differences among any two data set-based methods in nine regions of Wenzhou were conducted, and the overall level of agreement of flooded area lies between 79% to 93%, while the overall level of agreement of lodged area lies between 64% to 88%. The detailed cross-comparisons of flooded and lodged paddy rice areas in the nine regions of Wenzhou are shown in Fig. 9.

4 Discussion

4.1 Detection of lodged and flooding paddy rice

In this study, we proposed a method to detect two main kinds of typhoon-derived disasters of paddy rice: flooding and lodging. Sentinel-1 backscattering images in both typhoon and non-typhoon-effected seasons were used to obtain *RNDFI* and *RNDLI* values which are designed to identify and extract flooded and lodged rice after the passage of typhoon. Meanwhile, vegetation indices (*NDVI*, *EVI*) derived from Sentinel-2 data, were also used to verify the proposed indices. The results show that both microwave and optical remote sensing data can be successfully employed to estimate the spatial extent of flooded and lodged rice. CD and thresholding methods, operated within the GEE platform resulted in a more efficient and objective detection of rice damage. However, due to the limitations

Table 4 Confusion matrixes of land cover classification accuracy

	VH + *NDVI*-based				
Classes	paddy rice	water	urban	forest	others
paddy rice	106	0	0	1	4
water	2	40	0	0	0
urban	0	0	32	0	0
forest	0	1	2	38	1
others	3	1	2	0	13
UA (%)	95	95	100	90	68
PA (%)	95	95	89	97	72
Overall Accuracy:93% Kappa Statistic:0.9					
	VH + *NDVI*-based				
	paddy rice	water	urban	forest	others
paddy rice	102	2	0	2	5
water	3	36	2	1	0
urban	0	0	32	0	0
forest	7	2	0	33	1
others	5	0	2	5	7
UA (%)	92	86	100	77	37
PA (%)	87	90	89	80	54
Overall Accuracy:85% Kappa Statistic:0.8					

PA and UA are producer's accuracy and user's accuracy, respectively

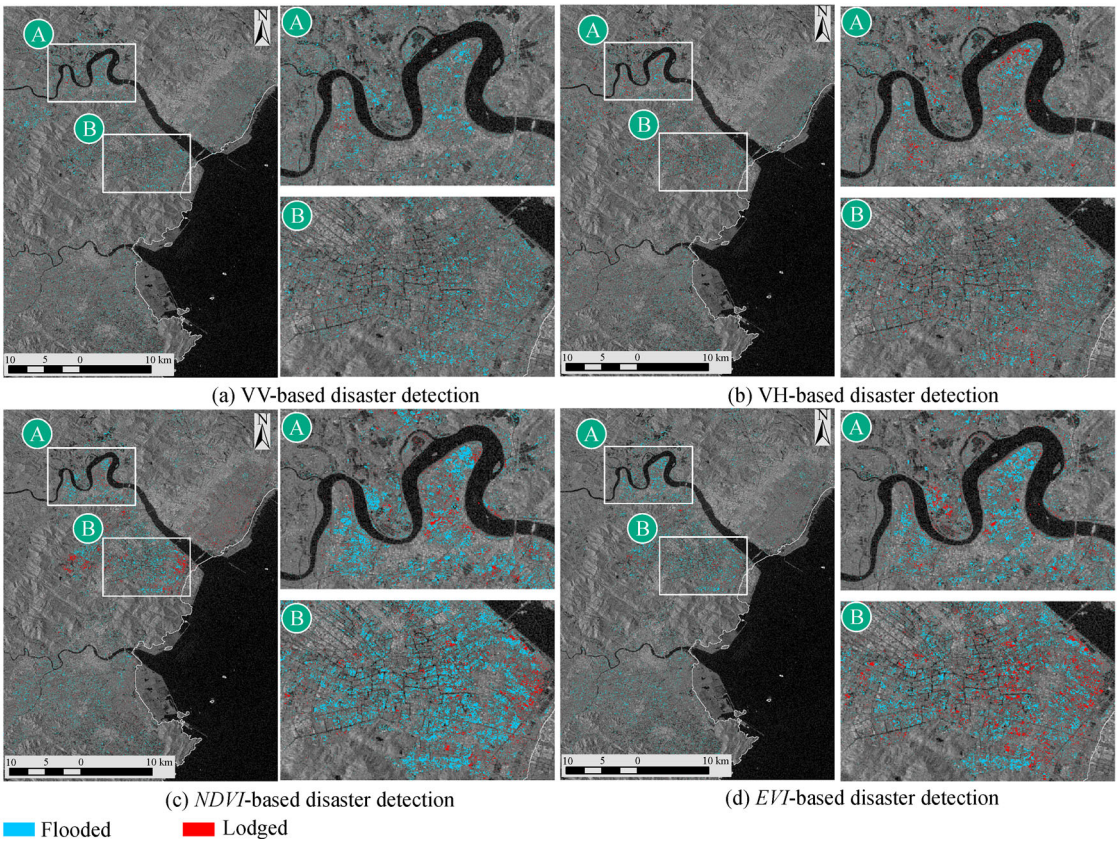

Fig. 7 (a) VV-based, (b) VH-based, (c) *NDVI*-based, and (d) *EVI*-based flooding and lodging areas in paddy rice fields.

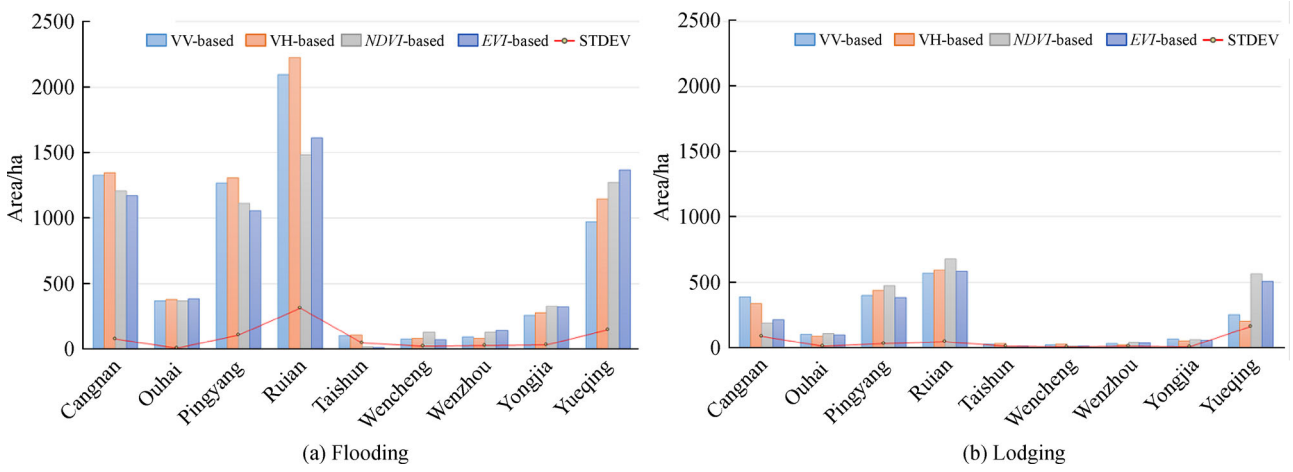

Fig. 8 (a) Flooded and (b) lodged area statistics in nine regions of the study area compared for VV-based, VH-based, *NDVI*-based and *EVI*-based methods. The red line in the figure show the standard deviation of four different results.

Table 5 Paddy rice flooding and lodging area of nine regions in the study area using VV-based, VH-based, *NDVI*-based and *EVI*-based methods

Region	Flooded area /ha				Lodged area /ha			
	VV	VH	*NDVI*	*EVI*	VV	VH	*NDVI*	*EVI*
Cangnan	1325.06	1345.27	1206.18	1173.07	388.75	338.2	187.37	212.36
Ouhai	368.5	377.2	365.59	379.98	103.14	86.37	104.69	94.38
Pingyang	1267.64	1304.9	1111.81	1055.06	396.2	437.81	471.43	382.83
Ruian	2096.22	2222.89	1484.34	1612.69	570.83	596.7	677.8	584.3
Taishun	100.87	108.74	146.1	112.49	25.45	30.8	0.959	8.64
Wencheng	73.96	82.37	127.47	73.65	21.869	24.53	8.759	10.18
Wenzhou	90.9	79.01	128.44	139.87	28.65	19.82	41.98	36.95
Yongjia	255.87	276.73	325.63	323.9	65.881	52.08	62.05	58.05
Yueqing	969.6	1146.16	1271.7	1367.51	251.11	200.91	565.25	510.92
Sum	6548.62	6943.27	6035.77	6136.99	1851.91	1787.22	2120.32	1898.61

of field observations, the parameters we used for thresholding were based on previous research (Long et al., 2014; Cian et al., 2018), which may affect computational accuracy.

4.2 The influence of data quality on the experimental results

Because typhoons are often accompanied by strong winds and rainstorms, the quality of optical data are greatly affected by the weather conditions. In this case, the affected area of rice extracted from Taishun, Wencheng, Wenzhou, Yueqing and other areas is not completely consistent with the results of microwave data extraction, which is likely due to sub-optimal quality of the Sentinel-2 data (Yesou et al., 2016). On the other hand, Sentinel-1 data have higher spatial and temporal resolution and, moreover, are not affected by clouds. Sentinel-1 therefore has excellent potential in the evaluation of disasters during bad weather conditions (Amitrano et al., 2018). We hope to merge more optical and microwave data sourced from different sensors to assess rice disasters in future research, so as to solve the problem of lack of data in earlier years.

5 Conclusions

In this study we propose a new method of mapping flooded and lodged area of paddy rice during the passage of a typhoon based on multi-temporal Sentinel-1 and Sentinel-2 data series with the aid of the GEE cloud computing platform. Two indices are proposed for flooded and lodged paddy rice detection, where *RNDFI* is used to map flooded pixels, and *RNDLI* is used to map lodged pixels.

The proposed method has the following advantages: i) indices and threshold-based detection methods facilitate the accurate detection of both flooded and lodged paddy

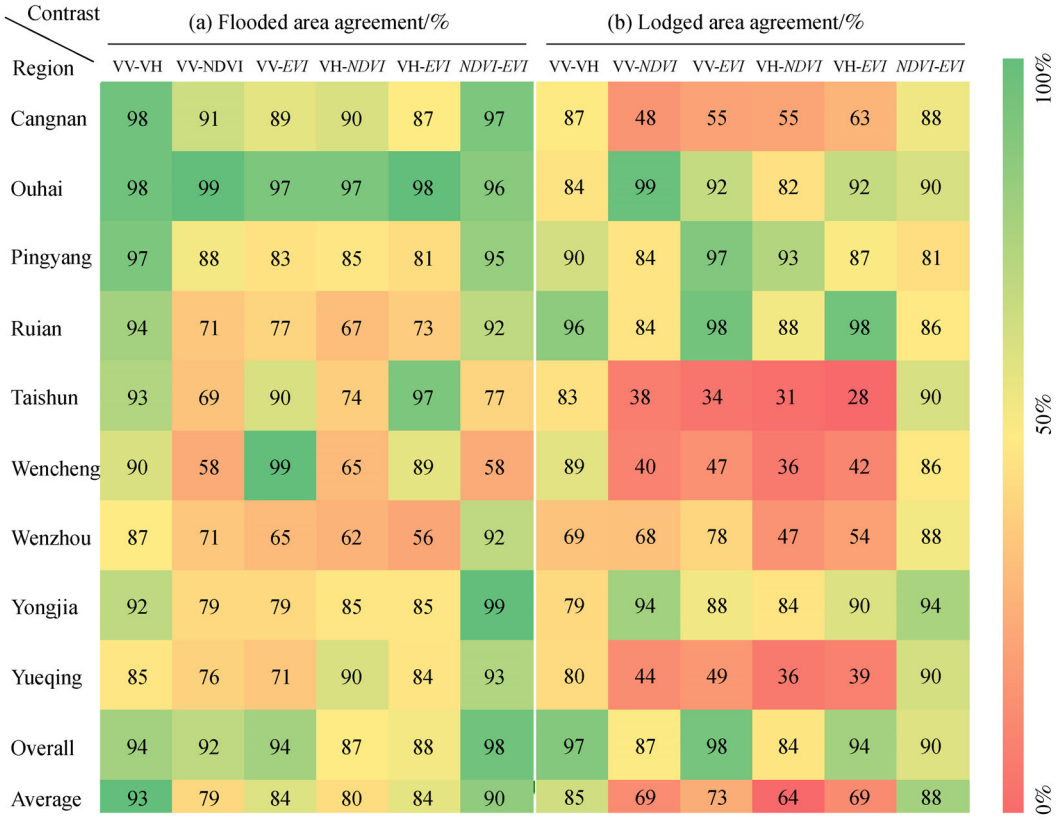

Fig. 9 (a) and (b) show the cross-comparison of flooded and lodged paddy rice area based on four different data sets, Sentinel-1-derived VV and VH backscattering coefficient, Sentinel-2-derived *NDVI* and *EVI*, respectively.

rice pixels in an automated way; ii) GEE makes it possible to deal with the very large data sets involved and to retrieve the results in a few minutes; this facilitates real-time extraction of relevant information during or following a disaster; iii) the data from the same growth stage of rice in recent years are used for CD and enable the construction of maps of flooded and lodged paddy rice areas which largely eliminates errors of backscatter or reflectance changes caused by the growth phases of the paddy rice itself.

There are, nevertheless, some limitations of the proposed method. Changes in rice planting during the year, such as abandoning or changing crop cultivation, may lead to misrepresentation of extracted flooded and lodged area results. Further refinements should include: i) long-term monitoring of rice crop disasters to assess post-disaster recovery, and ii) the effects of flooding and lodging on rice yield should be analyzed so that the yield reduction caused by extreme weather events can be more accurately estimated.

Acknowledgements This study was supported by the National Basic Research Program of China (No. 2015CB452806), the National Natural Science Foundation of China (Grant No. 41271055), the Shanghai Agriculture Applied Technology Development Program (No. G2014070402), and Shanghai Science and Technology Committee (No. 17DZ1205300). The computation was supported by the ECNU Multifunctional Platform for Innovation (001). Prof. Jiong Shu is thanked for many valuable suggestions in the revision of the manuscript.

References

Amitrano D, Martino G, Iodice A (2014). Sentinel-1 for monitoring reservoirs: a performance analysis. Remote Sens, 6(11): 10676–10693

Balzter H, Cole B, Thiel C, Schmullius C (2015). Mapping CORINE land cover from Sentinel-1A SAR and SRTM digital elevation model data using random forests. Remote Sens, 7(11): 14876–14898

Bouman B A M, Hoekman D H (1993). Multi-temporal, multi-frequency radar measurements of agricultural crops during the Agriscatt-88 campaign in the Netherlands. Int J Remote Sens, 14(8): 1595–1614

Bouvet A, Le Toan T, Lam-Dao N (2009). Monitoring of the rice cropping system in the Mekong Delta using ENVISAT/ASAR dual polarization data. IEEE Trans on Geosci and Remote Sens, 47(2): 517–526

Cian F, Marconcini M, Ceccato P (2018). Normalized Difference Flood Index for rapid flood mapping: taking advantage of EO big data. Remote Sens Environ, 209: 712–730

Drusch M, Del Bello U, Carlier S, Colin O, Fernandez V, Gascon F, Hoersch B, Isola C, Laberinti P, Martimort P, Meygret A, Spoto F, Sy O, Marchese F, Bargellini P (2012). Sentinel-2: ESA's optical high-

resolution mission for GMES operational services. Remote Sens Environ, 120: 25–36

Fu B, Wang Y, Campbell A, Li Y, Zhang B, Yin S, Xing Z, Jin X (2017). Comparison of object-based and pixel-based Random Forest algorithm for wetland vegetation mapping using high spatial resolution GF-1 and SAR data. Ecol Indic, 73: 105–117

Gorelick N, Hancher M, Dixon M, Ilyushchenko S, Thau D, Moore R (2017). Google Earth Engine: Planetary-scale geospatial analysis for everyone. Remote Sens Environ, 202: 18–27

Hansen M C, Potapov P V, Moore R, Hancher M, Turubanova S A, Tyukavina A, Thau D, Stehman S V, Goetz S J, Loveland T R, Kommareddy A, Egorov A, Chini L, Justice C O, Townshend J R (2013). High-resolution global maps of 21st-century forest cover change. Science, 342(6160): 850–853

Kwak Y, Arifuzzanman B, Iwami Y (2015). Prompt proxy mapping of flood damaged rice fields using MODIS-derived indices. Remote Sens, 7(12): 15969–15988

Lasko K, Vadrevu K P, Tran V T, Justice C (2018). Mapping double and single crop paddy rice with Sentinel-1A at varying spatial scales and polarizations in Hanoi, Vietnam. IEEE J Sel Top Appl Earth Obs Remote Sens, 11(2): 498–512

Lee K S, Lee S I (2003). Assessment of post-flooding conditions of rice fields with multi-temporal satellite SAR data. Int J Remote Sens, 24 (17): 3457–3465

Liu D, Pang L, Xie B (2009). Typhoon disaster in China: prediction, prevention, and mitigation. Nat Hazards, 49(3): 421–436

Mateo-García G, Gómez-Chova L, Amorós-López J, Muñoz-Marí J, Camps-Valls G (2018). Multitemporal cloud masking in the Google Earth Engine. Remote Sens, 10(7): 1–18

Mentaschi L, Vousdoukas M I, Pekel J F, Voukouvalas E, Feyen L (2018). Global long-term observations of coastal erosion and accretion. Sci Rep, 8(1): 12876

Mutanga O, Kumar L (2019). Google Earth Engine applications. Remote Sens, (11): 1–4

Nguyen D B, Gruber A, Wagner W (2016). Mapping rice extent and cropping scheme in the Mekong Delta using Sentinel-1A data. Remote Sens Lett, 7(12): 1209–1218

Pekel J F, Cottam A, Gorelick N, Belward A S (2016). High-resolution mapping of global surface water and its long-term changes. Nature, 540(7633): 418–422

Sakagami J I, Kawano N (2011). Survival of submerged rice in a flood-prone region of West Africa. Tropics, 20(2): 55–66

Setter T L, Laureles E V, Mazaredo A M (1997). Lodging reduces yield of rice by self-shading and reductions in canopy photosynthesis. Field Crops Res, 49(2–3): 95–106

Son N T, Chen C F, Chen C R, Minh V Q (2018). Assessment of Sentinel-1A data for rice crop classification using random forests and support vector machines. Geocarto Int, 33(6): 587–601

Tian X, Zou X (2018). NOAA-20 and S-NPP ATMS Captures warm-core evolution of Typhoon Maria. In: AGU Fall Meeting Abstracts

Torres R, Snoeij P, Geudtner D, Bibby D, Davidson M, Attema E, Potin P, Rommen B Ö, Floury N, Brown M, Traver I N, Deghaye P, Duesmann B, Rosich B, Miranda N, Bruno C, L'Abbate M, Croci R, Pietropaolo A, Huchler M, Rostan F (2012). GMES Sentinel-1 mission. Remote Sens Environ, 120: 9–24

Wakabayashi H, Motohashi K, Kitagami T, Tjahjono B, Dewayani S, Hidayat D, Hongo C (2019). Flooded area extraction of rice paddy field in Indonesia Using Sentinel-1 SAR Data. Int Arch Photogramm Remote Sens Spat Inf Sci, 42(W7): 3–7

Wang Y, Colby J D, Mulcahy K A (2002). An efficient method for mapping flood extent in a coastal floodplain using Landsat TM and DEM data. Int J Remote Sens, 23(18): 3681–3696

Xia D R, Wu J K (2017) Current situation analysis and development suggestions of rice production and varieties in Wenzhou City from 2007 to 2016. China Seed Industry, 2017 (12): 36–39 (in Chinese)

Xiao X, Boles S, Liu J, Zhuang D, Frolking S, Li C, Salas W, Moore B III (2005). Mapping paddy rice agriculture in southern China using multi-temporal MODIS images. Remote Sens Environ, 95(4): 480–492

Yang M D, Huang K S, Kuo Y H, Tsai H, Lin L M (2017). Spatial and spectral hybrid image classification for rice lodging assessment through UAV imagery. Remote Sens, 9(6): 583

Yesou H, Pottier E, Mercier G, Grizonnet M, Haouet S, Giros A, Faivre R, Huber C, Michel J (2016) Synergy of Sentinel-1 and Sentinel-2 imagery for wetland monitoring information extraction from continuous flow of sentinel images applied to water bodies and vegetation mapping and monitoring. In: 2016 IEEE International Geoscience and Remote Sensing Symposium (IGARSS). IEEE, 2016: 162–165